Hindawi
Journal of Spectroscopy
Volume 2022, Article ID 7526826, 12 pages
https://doi.org/10.1155/2022/7526826

*Research Article*

# Study on the Quantitative Assessment of Impact Damage of Yellow Peaches Using the Combined Hyperspectral Technology and Mechanical Parameters

**Feng Zhang, Bin Li, Hai Yin, Jiping Zou, and Aiguo Ouyang**

*Institute of Optical-Electro-Mechatronics Technology and Application, East China Jiao Tong University, National and Local Joint Engineering Research Center of Fruit Intelligent Photoelectric Detection Technology and Equipment, Nanchang 330013, China*

Correspondence should be addressed to Aiguo Ouyang; ouyang1968711@163.com

Received 25 June 2022; Revised 21 September 2022; Accepted 23 September 2022; Published 14 October 2022

Academic Editor: Daniel Cozzolino



The quantitative description of the impact damage of yellow peaches is an essential basis for evaluating their quality and guiding their postharvest handling. In this study, the combined hyperspectral technology and mechanical parameters method were used to quantitatively investigate the impact damage of yellow peaches. Firstly, the mechanical parameters, which are damaged area, absorbed energy, maximum contact force, and maximum stress of yellow peaches, were obtained by the impact device. The statistical regression models between mechanical parameters and damage area were established, and the results showed that the absorbed energy and maximum contact force are the optimal parameters to characterize the impact damage of yellow peaches. Then, the raw spectra were preprocessed by three spectral pretreatment methods, which are standard normal variate (SNV), multiplicative scatter correction (MSC), and SG smoothing, respectively, and the feature wavelengths were selected by the competitive adaptive reweighted sampling (CARS), and the quantitative relationships between spectra and mechanical parameters were successfully modeled based on partial least squares regression (PLSR). The results showed that there is a strong linear correlation between the spectral data and the mechanical parameters, and the prediction performance of the SNV-CARS-PLSR model is best, and the RP and RMSEP of the damaged area, absorbed energy, maximum contact force, and maximum stress of it were 0.920 and 86.452 $mm^2$, 0.845 and 1.303 J, 0.943 and 49.666 N, 0.660 and 0.146 MPa, respectively. In a word, this study shows that the combined hyperspectral technology and mechanical parameters method can be used to quantitatively assess the impact damage of yellow peaches, and guide the postharvest handling of fruits.

## 1. Introduction

Yellow peaches are rich in nutrition and can be consumed regularly to improve immunity, and the risk of chronic diseases can be reduced by it. However, yellow peaches are inevitably subjected to mechanical damage during harvesting, processing, packaging, and transporting [1, 2]. According to the relevant literature, the impact damage caused by the impact forces between fruits or between fruits and equipment during harvest, transporting, and processing is the most common type of mechanical damage to fresh fruits [3, 4]. The bruising of fresh fruit dramatically reduces its quality, which leads to economic losses for farmers. Although fruit bruises can be detected by advanced machines and the damaged fruit can be discovered and it can be picked out in time, the incidence of impact damage is not reduced by this method. Thus, preventive measures should be taken during packing, transporting, and processing to reduce the incidence of fruit bruises [5, 6]. Therefore, it is critical to analyse the mechanical properties of fruits.

Mechanical parameters such as maximum force, maximum stress, average pressure, absorbed energy, restitution coefficient, impact velocity, and acceleration are the main parameters in characterizing the degree of impact damage of fruits [7–9]. Strope and Gołacki [10] designed a fruit collision device based on the principle of the single pendulum

to record the maximum force, maximum stress, and permanent deformation of apples when they were impacted. It was discovered that permanent deformation and maximum stress were the optimum parameters for assessing impact damage to apples. An et al. [11] investigated the damage mechanism of the internal structure of strawberries. They found that the absorbed energy was an appropriate and easily measurable mechanical parameter for evaluating the damage degree of strawberries. However, these research studies only analyzed the correlation between the different mechanical parameters and the degree of impact damage of fruits, and the quantitative prediction of the impact damage degree of fruits has not been achieved. Hence, it is essential to find a method to quantitatively evaluate and predict the degree of impact damage on fruits.

In recent years, with the emergence and development of hyperspectral technology, more and more researchers have used hyperspectral technology to detect the internal quality and external damage of fresh fruits [12]. Hyperspectral is a fast and nondestructive technique that integrates spectroscopic and imaging technologies to provide spectral and spatial information about the object being detected simultaneously [13, 14]. Tan et al. [15] used spectral data to establish a classification model of different damage levels of apples. Zhao et al. [16] used combined hyperspectral technology and finite element analysis to build a visualization model of bruised Goji berries. The hyperspectral technology can also be used to detect the fungal contamination in strawberries [17], the hollowness classification of white radish [18], common defects in citrus [19], and black spots on potatoes [20]. To detect fruit bruises, many researchers have established bruise classification models for various fruits by associating hyperspectral information with the physicochemical properties of fruits (e.g., soluble solids, titratable acids, flesh color, and hardness) [21–24]. But these models only distinguish whether the fruit was damaged. Meanwhile, Zhang et al. [25] used the hyperspectral imaging technique within the wavelength range of 900–1700 nm to quantitatively investigate the impact damage of apples, and the PLSR model was established. Xu et al. [26] used a pressure-sensitive film technique to measure the mechanical parameters and collected hyperspectral data of apples in the range of 900–1700 nm to establish a quantitative prediction model of the mechanical parameters for apples. However, on the one hand, they use a collision device based on the free fall principle to measure the mechanical parameters of apples, the impact area of apples is not always located at its equatorial zone during free fall, and the pressure-sensitive film has a buffering effect on the apple impact process, which lead to increasing the measurement error of the mechanical parameters; on the other hand, using hyperspectral imaging to quantify the impact damage to yellow peaches is rarely reported.

Therefore, the combined hyperspectral technology within the wavelength range of 397.5–1014 nm and mechanical parameters method is proposed to quantitatively investigate the impact damage of yellow peaches. Firstly, in order to reduce the measurement error of mechanical parameters of fruits, the new collision device, which contains a single pendulum mechanism, a high-speed camera, and an intelligent data acquisition system (DASP-V11), is designed, and the mechanical parameters of yellow peach impact damage are obtained by it. Then, the statistical regression models between mechanical parameters and damage area are established to find the optimal mechanical parameters characterizing the impact damage of yellow peaches. Finally, the PLSR model between spectral variables and mechanical parameters is established to quantify and predict the impact damage of yellow peaches.

## 2. Material and Methods

*2.1. Yellow Peach Samples.* All samples in this study are "Dangshang" yellow peach and they were stored at 4°C for less than 2 weeks after their harvest. A total of 180 fresh, undamaged, and regularly shaped yellow peaches were used in this experiment. To reduce the influence of the weight and curvature radius of the yellow peaches on the bruise size, the average weight of samples was about $248 \pm 5$ g, and the equatorial diameter was about 78 mm. Before the collision experiments, all yellow peaches were cleaned and numbered. They were placed in a room with 20°C and 40% relative humidity for 24 hours to minimize the effect of fruit temperature on impact damage. All samples were randomly divided into 6 groups. In order to obtain different degrees of impact damage, 6 groups of samples were released from angles of 30°, 40°, 50°, 60° 70°, and 80°.

*2.2. Collision Device and Measurement Instrument.* The fruit impact device used in this paper is designed based on the single pendulum principle, and its structure is shown in Figure 1. The device consists of a support frame and a base, on which there is a removable flat plate underneath the base, and the pressure sensor (Cheng Ying Sensor Co., Bengbu, China) is mounted on the flat plate. The pendulum arm was made of 80 cm of nonextendable fishing line, and the fruit jig was made of a new material, polylactic acid (PLA), by a 3D printer. The weight of both the fruit jig and fish line is so small that it can be negligible; therefore, the effect of the mass of the jig and rotational inertia generated by the swing arm can be ignored. When the pendulum arm was moved to the lowest point, the pendulum arm was parallel to the support frame in the vertical direction, which ensured that the impact force was perpendicular to the impact surface and the center collision condition of the force sensor was met. The device also has a fixed protractor, and the controlled angle of the pendulum arm was from 5° to 85°. After each test sample impacts the pressure transducer, the sample was grabbed by hand to prevent a second impaction. The force response during the collision can be measured by means of a pressure sensor, model HZC-H1, with a sensitivity of 2.00 mV/N and a measurement range of 0–100 kg.

Two systems were used to collect the mechanical parameters of the experiment. The intelligent data acquisition apparatus (DASP-V11, Coinv, China) was connected to the force transducer, and it could record the force response process in time; the collected data were calculated and

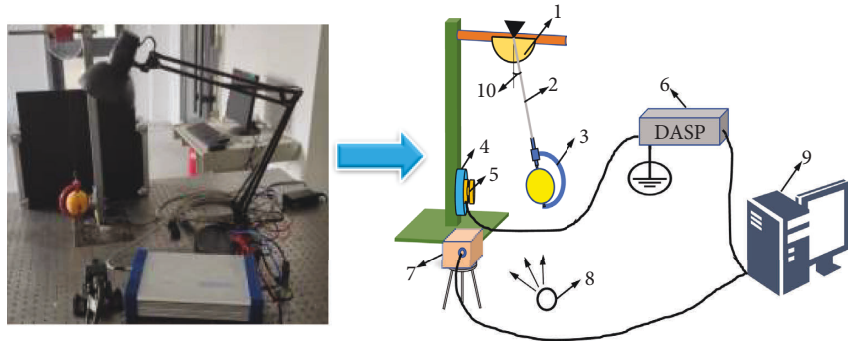


Figure 1: Structure diagram of the impact device: 1-protractor, 2-pendulum arm, 3-fruit fixture, 4-dynamic bumper plate, 5-pressure sensor, 6-intelligent data acquisition and signal processing, 7-high-speed camera, 8-light source, 9-PC, 10-release angle.

analyzed by relevant software of DASP-V11, and the mechanical parameters such as maximum contact force and average force can be obtained; The sampling frequency of force was 51.2 kHz, and the calibration value was 0.02 mV/N, and the measurement was triggered when the contact force was greater than 0.5 N. The high-speed digital camera (HXC20NIR, Hamamatsu, Japan) and a lens with a constant focal length of 35 mm were used to capture the entire collision and bounce process, and the picture acquisition speed was set to 1000 frames/s. Due to the high shooting speed, the whole experiment needs to be illuminated by the high brightness and strobe-free LED lamp (Opple, Shanghai, China). In this experiment, the high-speed camera was placed on the lifting platform, which can be adjusted with an accuracy of 1 mm in both directions to reduce the measurement error caused by inaccurate camera positioning. In this impact test, the conversion from pixels to millimeters of image size was 0.130 mm/pixel.

### 2.3. Calculation and Measurement of Mechanical Parameters

*2.3.1. Damage Area.* After the impact experiment, in order to easily identify and measure the damaged areas of yellow peach, the samples were stored at 20°C for 24 hours [27]. In this experiment, the damaged region of all samples can be approximated as a circle. Thus, the diameters in two mutually perpendicular directions of the damaged area were measured by a digital vernier calliper (accuracy 0.01 mm) and the average of the two diameters was used as the diameter of the damaged yellow peach. The damaged area was calculated by formula (1)

$$A = \frac{\pi D^2}{4}, \tag{1}$$

where A is the damaged area ($mm^2$), $D$ is the bruise diameter (mm).

*2.3.2. Absorbed Energy.* Due to the plastic deformation of yellow peaches, some of the impact energy will be absorbed by the yellow peaches in the impact collision test. Ignoring the energy loss, the absorbed energy of the yellow peach is equivalent to the difference between the impact energy and the rebound energy; the higher the absorbed energy, the higher the damage caused to the fruits. Since the high-speed camera can acquire 1000 images in 1 s, the speed of the yellow peach was low at the time of impact and bounce. Therefore, the movement of the spatial position of the yellow peach in two consecutive frames of images was the displacement of the yellow peach in $\Delta t$ time (in this experiment, $\Delta t = 1 \times 10^{-3}$·s). The two connected frames of images before and after the collision were selected. The distance of the yellow peach moving in the picture was solved by the impixelinfo function in MATLAB R2018b [28, 29]. Hence, the impact velocity and rebound velocity of yellow peaches can be calculated by formula (2):

$$v = \frac{s}{t}, \tag{2}$$

where $S$ is the actual displacement of the yellow peach and $t$ is the time difference between the two connected frames of images ($t = 1/1000$ s). For the accuracy of the results, the velocity values of several points were solved in this study, and then they were averaged. After computing the velocity values of each yellow peach before and after the collision, the absorbed energy of the yellow peach can be calculated by formula (3).

$$\Delta E = \frac{1}{2} m\left(v_1^2 - v_2^2\right), \tag{3}$$

where $v_1$ is the velocity of yellow peach before the collision, $v_2$ is the velocity of yellow peach after the rebound, and $m$ is the mass of yellow peach.

*2.3.3. Maximum Contact Force and Maximum Stress.* The DASP-V11 was connected with the force sensor to record the force response process in real time. Then, the collected data were analyzed in the time domain by relevant software, and the maximum contact force at the time of collision of each yellow peach can be obtained. The whole collision process of the yellow peach was recorded by the high-speed camera. When the impact force reaches its maximum value, the contact width between the yellow peach collision surface and the force sensor could be determined by the photos taken by the high-speed camera, and the contact area at this time could be calculated by formula (4): [30].

$$A_{\text{cont}} = \frac{\pi w_{\text{cont}}^2}{4}, \tag{4}$$

where $A_{\text{cont}}$ is the contact area, $w_{\text{cont}}$ is the contact width. The maximum stress is calculated by formula (5):

$$\sigma_{\max} = \frac{F_{\max}}{A_{\text{cont}}}, \tag{5}$$

where $\sigma_{\max}$ is the maximum stress, $F_{\max}$ is the maximum force, and $A_{\text{cont}}$ is the contact area.

*2.4. Hyperspectral Images Acquisition and Extraction.* After the damaged peaches were left at a room temperature of 20°C for 24 hours, the hyperspectral images of the damaged surface of yellow peaches were acquired by the hyperspectral imaging system. The hyperspectral imaging acquisition system is shown in Figure 2. The system consists of an imaging spectrometer, a charged coupled device (CCD) camera, four halogen headlamps, and a moving platform. In this study, the wavelength range was 397.5–1014 nm, and the spectral resolution was 3.5 nm with 176 bands. The relevant parameters were set as follows: the distance between the camera lens and the sample was 48 cm, the exposure time was 6 ms, and the advancing speed of the moving platform was 3 cm/s.

Before data processing and analysis of the acquired hyperspectral images of yellow peaches, the reflectance of all raw spectral images needs to be calibrated in black and white due to dark currents and light inhomogeneities in the CCD camera. The white reference image was acquired by the camera capturing the white calibration plate, and the image when the lens was obscured entirely was captured as the black reference image. The calibration images were calculated by formula (6):

$$\mathrm{I} = \frac{\mathrm{I}_r - \mathrm{I}_d}{\mathrm{I}_w - \mathrm{I}_d}, \tag{6}$$

where $I_r$ is the original hyperspectral image, $I_d$ is the dark reflection image, and $I_w$ is the white reflection image. A rectangular region of interest (ROI) was selected in the yellow peach damage area and the average spectral value of the ROI region was calculated using ENVI4.5 software.

*2.5. Spectral Pretreatment.* The quality of the information of the damaged area is reflected by the raw spectra. But, in collecting the raw spectra, the sample state, instrument performance, and other external environmental disturbances may introduce information which is not relevant to the quality of the damaged area, such as system noise and ambient stray light. There is not a standard about which is the best type of pretreatment for spectra [31]. Therefore, it is necessary to use different methods to pretreat the original spectra so that an appropriate preprocessing method can be selected. In this study, the standard normal variate (SNV) transformation, multiplicative scatter correction (MSC), and SG smoothing are used to pretreat original spectra, respectively.

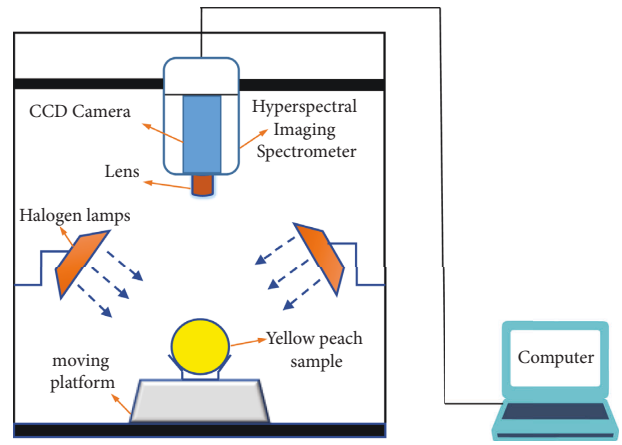


Figure 2: Schematic illustration of the hyperspectral imaging system.

*2.6. Characteristic Wavelength Selection.* The data processing rate is slowed down by a large amount of full-spectrum wavelength data. The redundancy and covariance of adjacent wavelength data points and the online application of hyperspectral imaging technology are limited. Therefore, the feature extraction algorithm is needed to select the most representative feature wavelengths from the full-band spectrum to meet the requirements of fast detection. In this study, the competitive adaptive reweighted sampling (CARS) method was used to select the characteristic wavelengths.

The CARS is a feature wavelength selection method based on Monte Carlo sampling with PLS model regression coefficients [32]. The variables with larger absolute values of regression coefficients in the PLS model are selected by the adaptive reweighting technique (ARS) and exponential decay function (EDF). Then the variables in the subset of PLS models with the smallest RMSECV are selected as the characteristic wavelengths by cross-validation. The main steps for selecting the characteristic wavelengths are described in detail in subsequent sections of this paper.

*2.7. Partial Least Squares Regression (PLSR).* The method of partial least squares regression (PLSR) is one of the most commonly used methods in quantitative analysis. The method incorporates principal component analysis and typical correlation on the basis of ordinary multiple regression, and the problem of multicollinearity of independent variables can be solved by it [33]. The choice of the number of principal components is very important in the modelling process, where PLSR model performance is strongly affected. Underfitting will occur if the number of principal components is too small. If too many principal components are selected, overfitting will occur. Therefore, the optimal number of principal components can be selected by cross-validation.

It is difficult to obtain an ideal sample set from a randomly selected sample. Currently, the most commonly used sample selection method is the Kennard-Stone (KS) method. The KS method can uniformly select samples in the feature

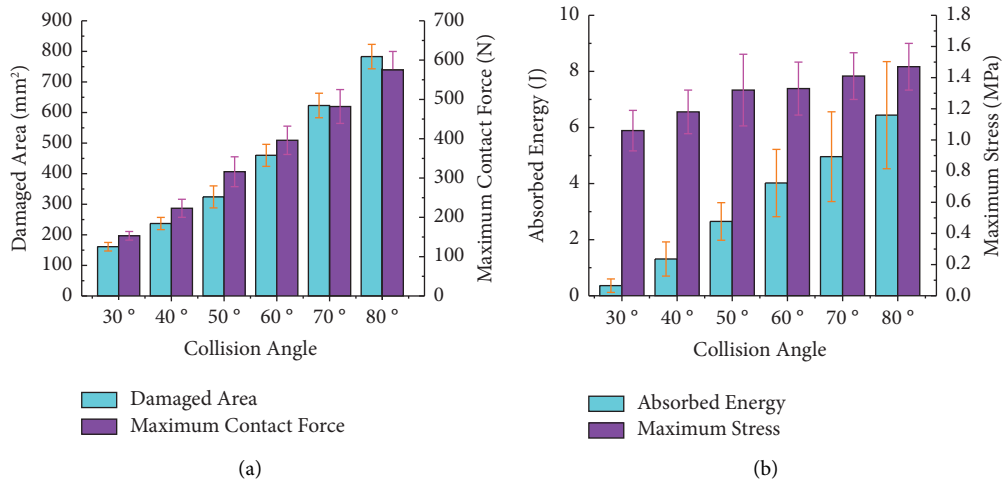


FIGURE 3: Changes in mechanical parameters of yellow peach at different collision angles: (a) Damage area and maximum contact force; (b) Absorbed energy and maximum stress.

space based on the Euclidean distance between variables. Therefore, the KS method is used to select 20 samples from each release angle, with a total of 120 samples selected as the modelling set and the remaining 60 samples selected as the prediction set in this study. The PLSR models of damage area, absorbed energy, maximum contact force, and maximum stress were built, respectively.

The main metrics used to evaluate the performance of the PLSR model are the modelling set correlation coefficient ($R_C$), the root mean square error of the modelling set (RMSEC), the prediction set correlation coefficient ($R_P$), and the root mean square error of the prediction set (RMSEP). The closer the correlation coefficient ($R$) is to 1, the more stable the model is, and the smaller the root mean square error (RMSE) is, the more accurate the model is. In addition, the results are compared based on RPD values, a greater value of RPD can be considered as a good prediction.

## 3. Results and Discussion

*3.1. Measurement Results and Statistical Analysis of Mechanical Parameters.* Figure 3 shows the measured results of the mechanical parameters of yellow peaches at 6 different release angles. As can be seen from Figures 3(a) and 3(b), the damage area, absorbed energy, maximum contact force, and maximum stress all gradually increase with the angle of release of yellow peach increasing. The greater the angle of release is, the more severe the impact damage to the yellow peach is. As can be seen from the error bars in the graph, the values of mechanical parameters show some volatility. After analysis, there are two main factors: on the one hand, the values of mechanical parameters are influenced by the physiological characteristics of the yellow peaches themselves, such as the hardness of the flesh, the radius of curvature, and the heterogeneity of the internal structure; on the other hand, they are influenced by external factors such as the oscillating attitude of the yellow peaches in the air, the position of the collision, the vibration of the support frame, and the system error. However, each mechanical parameter shows a certain linear variation with the release angle increasing, which indicates that it is feasible and reasonable to characterize yellow peaches' degree of impact damage by mechanical parameters.

Figure 4 shows the results of linear regression analysis of the mechanical parameters of yellow peaches. Damage area is the most intuitive parameter to characterize the extent of impact damage to yellow peaches. In this study, a statistical regression model was developed to investigate the quantitative relationship between mechanical parameters and the damaged area of yellow peaches, the damaged area is used as the dependent variable and mechanical parameters are used as the independent variables, so as to indirectly identify the optimal mechanical parameters characterizing the degree of impact damage to yellow peaches. From Figures 4(a) and 4(b), it can be seen that the absorbed energy and maximum contact force of samples have well linear correlations with the damaged area, and the $R^2$ is 0.83 and 0.90, respectively, which indicates that the absorbed energy and maximum contact force are the optimal mechanical parameters to characterize the impact damage of yellow peaches.

Figure 4(c) shows that the linear fit between the maximum stress and the damage area is not satisfactory. This is consistent with the findings of Lewis et al. [1] and Lu et al. [34]. After analysis, there are two possible reasons for this: firstly, there are certain differences in the firmness, radius of curvature, and mass of each yellow peach itself, which leads to a large error in the contact area of the yellow peach when the contact force reaches its maximum during the collision, resulting in an inaccurate calculation of the maximum stress. Secondly, from a material science perspective, the location of the maximum stress is randomly distributed, and it can only represent the stress value at a certain location on the damaged surface of the yellow peach, and the changing pattern of the whole damaged area cannot be reflected by it. Therefore, the use of maximum stress alone does not provide a satisfactory evaluation of the impact damage degree. In future work, the influence of the properties of the fruit itself

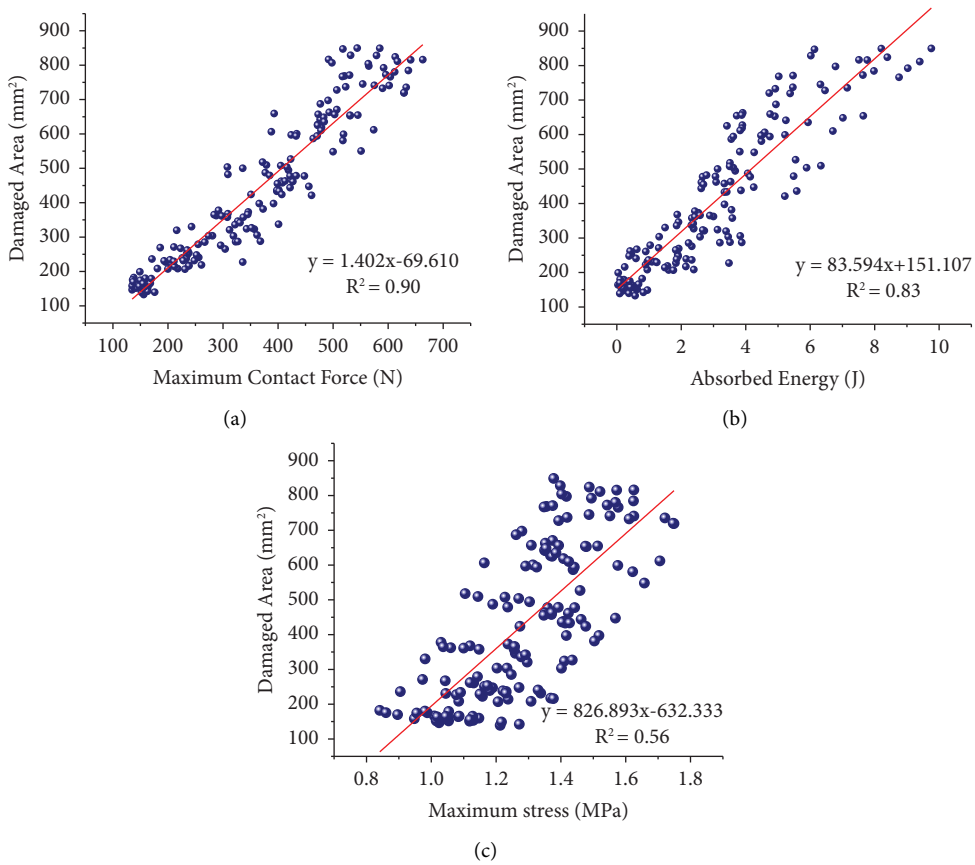


Figure 4: Statistical analysis of mechanical parameters of yellow peach: (a) Damage area-maximum contact force; (b) Damage area-absorbed energy; (c) Damage area-maximum stress.

on the experimental or the combination of the maximum stress with other mechanical parameters will be further controlled to assess the impact damage of the fruit.

*3.2. Spectral Characteristics Analysis.* Figure 5 shows the average spectra of yellow peach samples at six different collision angles. As can be seen from Figure 6, all the average spectral curves show distinct troughs at 704 nm and 995 nm, where the trough at 704 nm is due to the vibrational contraction of the C-H bond in the carbohydrate, and the trough at 995 nm is due to the O-H bond in the water molecule [35]. Specifically, impact damage can cause tissue damage and cell rupture in yellow peaches. After cell rupture, enzymes and water molecules are released, resulting in the light scattering in the damaged fruit tissue changing. Hence, the reflectivity of damaged yellow peaches displays differences. The average spectral reflectance of the damaged yellow peaches is significantly lower than the average spectral reflectance of the healthy yellow peaches. This is consistent with the finding that the water content of damaged areas of fruits is usually higher than that of normal tissues [36]. In addition, the samples of different degrees have similar spectral curve trends, but their spectral reflectance is obviously different in the same band; the more severely damaged the yellow peaches are, the lower the spectral reflectance is. This indicates the degree of damage of yellow peaches can be

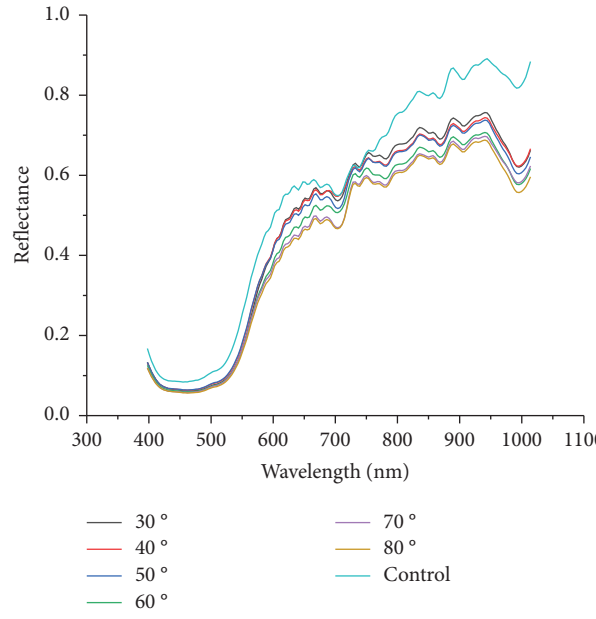


Figure 5: Average spectra of yellow peach samples at six different collision angles.

reflected by the average spectral curve. Therefore, this study will establish a prediction model between the spectral data and the mechanical parameters to quantitatively assess the

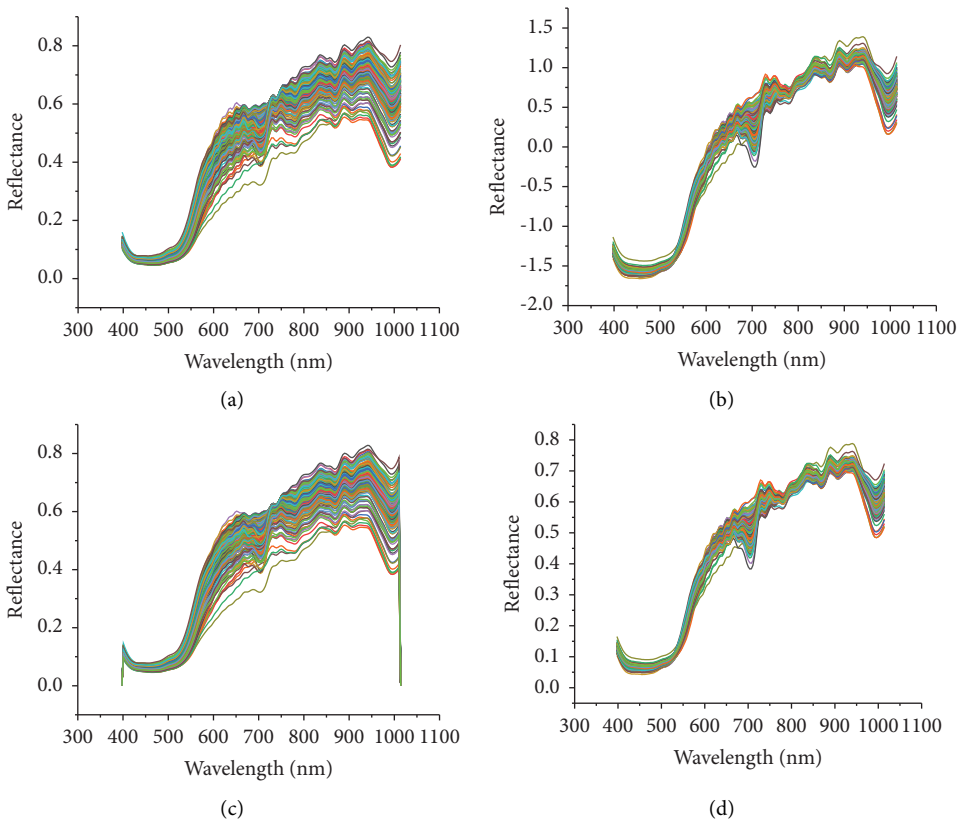


Figure 6: Spectra of all samples after being preprocessed: (a) Raw reflectance spectra; (b) SNV pretreatment; (c) SG pretreatment; and (d) MSC pretreatment.

extent of impact damage to yellow peaches. However, the average spectral curves of yellow peaches with different damage levels overlapped severely. Spectral data processing is needed to improve the modelling accuracy between the spectral data and the mechanical parameters.

*3.3. Results of Spectral Preprocessing.* Figure 6 shows the spectral curve after pretreatment by different methods. As it can be seen from Figure 6, although the pretreatment methods are different, the trend of the spectral curve is not basically changed. The position of the absorption peaks in the spectra is different, which is due to the different chemical content of each yellow peach damage region. As shown in Figure 6(c), there is no significant difference between the SG preprocessed spectra and the original spectra, it indicates that the SG preprocessing method does not filter out the noise information in the original spectra. The spectral curves in Figures 6(b) and 6(d) are more convergent and compact, indicating that after preprocessing by the SNV and MSC methods, small variations in the original spectral curves are amplified, while partially overlapping spectral signals are also separated. Overall, both the SNV and MSC methods are effective in removing the influence of scattering on spectral reflectance, and the spectral signal-to-noise ratio is improved. However, it is not straightforward to determine which pretreatment method is more effective from the spectral curve alone. Therefore, further analysis in conjunction with the modelling results is required.

The PLSR models are established based on raw spectral and preprocessed spectral data, respectively, and the results are shown in Table 1. The comparative analysis reveals that the different pretreatment methods have different effects on the performance of PLSR models with different mechanical parameters. Although the spectral curves after SNV and MSC pretreatment are basically same, for the prediction of damage area, absorbed energy, maximum contact force, and maximum stress, the $R_P$ and RMSEP of the SNV-PLSR model are 0.891 and 102.021 mm$^2$, 0.838 and 1.337 J, 0.907 and 70.319 N, and 0.664 and 0.145 MPa, respectively, and the values of RPD are 2.111, 1.521, 2.225, and 1.121, respectively. The $R_P$ and RMCEP of the MSC-PLSR model are 0.878 and 105.599 mm$^2$, 0.829 and 1.317 J, 0.901 and 69.961 N, and 0.641 and 0.148 MPa, respectively. The values of RPD are 1.923, 1.512, 2.224, and 0.966, respectively. The results show that the SNV-PLSR model's prediction performance is better than the MSC-PLSR model. It is worth noting that for the prediction of damage area, the $R_P$ and RMSEP of the Raw-PLSR model are 0.923 and 88.664 mm$^{2,}$, respectively, and the value of RPD is 2.583. It can be seen that the results of Raw-PLSR are better than those of SNV-PLSR in the prediction of the damaged area, but the prediction values of them are

Table 1: PLSR model prediction results of spectra after preprocessing with different methods.

| Spectral pretreat type | Parameter | PCs | Modeling set | | Prediction set | | |
|---|---|---|---|---|---|---|---|
| | | | RMSEC | $R_C$ | RMSEP | $R_P$ | RPD |
| Raw | DA ($mm^2$) | 8 | 83.515 | 0.925 | **88.664** | **0.923** | **2.583** |
| | AE (J) | 8 | 1.351 | 0.823 | 1.433 | 0.815 | 1.432 |
| | MCF (N) | 9 | 64.096 | 0.904 | 71.455 | 0.879 | 1.969 |
| | MS (MPa) | 8 | 0.162 | 0.699 | 0.147 | 0.642 | 0.954 |
| SNV | DA ($mm^2$) | 7 | 94.885 | 0.903 | 102.021 | 0.891 | 2.111 |
| | AE (J) | 13 | 1.271 | 0.849 | **1.337** | **0.838** | **1.521** |
| | MCF (N) | 11 | 62.520 | 0.909 | **70.319** | **0.907** | **2.225** |
| | MS (MPa) | 6 | 0.164 | 0.695 | **0.145** | **0.664** | **1.121** |
| MSC | DA ($mm^2$) | 7 | 93.509 | 0.905 | 105.599 | 0.878 | 1.923 |
| | AE (J) | 13 | 1.254 | 0.857 | 1.317 | 0.829 | 1.512 |
| | MCF (N) | 11 | 61.955 | 0.911 | 69.961 | 0.901 | 2.224 |
| | MS (MPa) | 7 | 0.162 | 0.695 | 0.148 | 0.641 | 0.966 |
| SG | DA ($mm^2$) | 9 | 82.974 | 0.926 | 91.779 | 0.920 | 2.559 |
| | AE (J) | 9 | 1.306 | 0.836 | 1.498 | 0.799 | 1.340 |
| | MCF (N) | 9 | 65.504 | 0.900 | 70.723 | 0.881 | 1.980 |
| | MS (MPa) | 8 | 0.161 | 0.696 | 0.155 | 0.614 | 0.887 |

DA: damaged area; AE: absorbed energy; MCF: maximum contact force; MS: maximum stress. PCs: the number of principal components. Bold values indicates the optimal prediction results for each mechanical parameter.

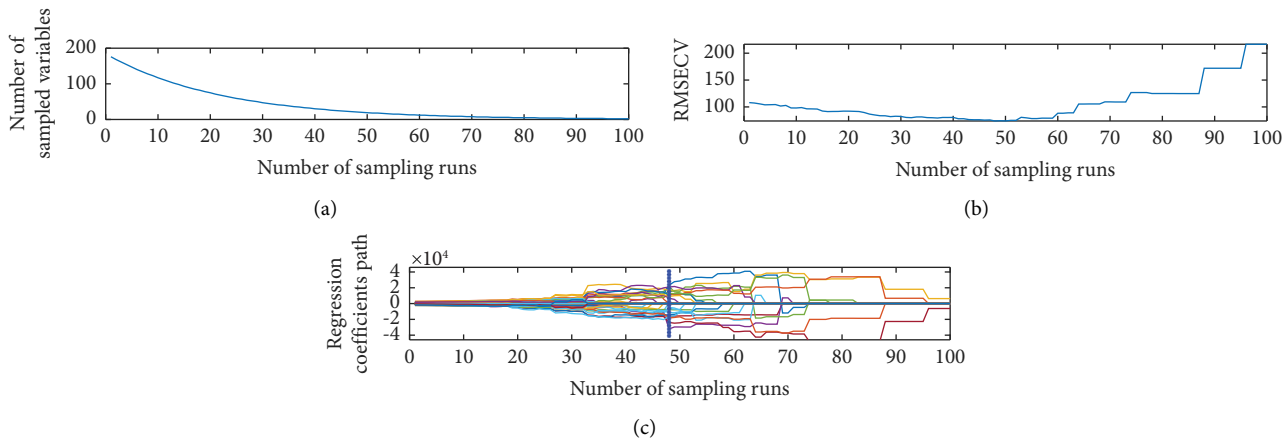


Figure 7: Variable selection based on CARS.

similar. In general, the raw spectra preprocessed by SNV is better. Therefore, the SNV preprocessed spectral data is used for the subsequent data analyses.

*3.4. Characteristic Wavelength Selection.* In this paper, the characteristic wavelengths of spectral data by SNV are extracted by CARS. In screening the characteristic wavelength of the mechanical parameters, the number of Monte Carlo samples is set to 100. Figure 7 shows the selection process of the characteristic wavelength of the damaged area. Figure 7(a) shows that the number of variables decrease as the number of samples increase, and the speed of variable reduction decreases from fast to slow due to the exponential decay function, indicating the selection process of variables is from "rough selection" to "exquisite selection." Figure 7(b) shows that the cross-validated values of RMSECV of PLS models decrease and then increase with the number of sampling operations as the number of sampling operations increase. The RMSECV value reaches the minimum value at the 48th sampling time, which indicates that the information is not related to the damaged area or the covariance has been removed in the 1–48th sampling operations. The RMSECV value increases after the 49th sampling operation, which indicates that the information related to the damaged area has been removed. Figure 7(c) represents the path of change in regression coefficients for 176 variables in the sample. The value of RMSECV based on the subset of variables obtained in the 48th sampling is minimized; thus, the variables obtained in the 48th sampling are designated as the characteristic wavelengths, which contain 21 variables, 441.3, 458.3, 468.3, 478.7, 533.4, 774.9, 792.7, 799.9, 803.4, 807, 810.6, 821.3, 828.5, 860.9, 864.5, 875.3, 889.8, 897.1, 904.3, 929.8, and 944.3 nm. In the latter study, these 21 wavelengths are used to predict further the damaged area of yellow peach instead of the full waveband.

The results of the characteristic wavelength selection for all mechanical parameters are shown in Table 2. As shown in Table 2, the number of characteristic wavelengths for

Table 2: The characteristic wavelength of different mechanical parameters selected by CARS.

| Parameters | Number of wavelengths | The selected characteristic wavelengths (nm) |
|---|---|---|
| DA ($mm^2$) | 21 | 441.3, 458.3, 468.3, 478.7, 533.4, 774.9, 792.7, 799.9, 803.4, 807, 810.6, 821.3, 828.5, 860.9, 864.5, 875.3, 889.8, 897.1, 904.3, 929.8, 944.3 |
| AE (J) | 9 | 595.6, 602.5, 606, 792.7, 807, 835.7, 846.5, 875.3, 889.8 |
| MCF (N) | 28 | 397.5, 441.3, 588.6, 606, 647.8, 675.8, 689.9, 696.9, 774.9, 792.7, 799.9, 803.4, 807, 810.6, 821.3, 835.7, 868.1, 871.7, 879, 882.6, 889.8, 897.1, 904.3, 922.5, 929.8, 944.3, 999.3, 1010.3 |
| MS (MPa) | 26 | 397.5, 512.8, 516.3, 519.7, 554.1, 619.9, 623.4, 647.8, 661.8, 665.3, 672.3, 682.9, 696.9, 807, 810.6, 839.3, 853.7, 897, 882.6, 886.2, 897.1, 900.7, 904.3, 940.7, 944.3, 959 |

Table 3: Prediction results of the PLSR model with different mechanical parameters based on the full waveband the characteristic wave band.

| Model | Parameter | PCs | Modeling set | | Prediction set | | |
|---|---|---|---|---|---|---|---|
| | | | RMSEC | $R_C$ | RMSEP | $R_P$ | RPD |
| SNV-PLSR | DA ($mm^2$) | 7 | 94.885 | 0.903 | 102.021 | 0.891 | 2.111 |
| | AE (J) | 13 | 1.271 | 0.849 | 1.337 | 0.838 | 1.521 |
| | MCF (N) | 11 | 62.520 | 0.909 | 70.319 | 0.907 | 2.225 |
| | MS (MPa) | 6 | 0.164 | 0.695 | **0.145** | **0.664** | **1.121** |
| SNV-CARS-PLSR | DA ($mm^2$) | 8 | 63.924 | 0.957 | **86.452** | **0.920** | **2.415** |
| | AE (J) | 8 | 1.214 | 0.863 | **1.303** | **0.845** | **1.622** |
| | MCF (N) | 14 | 46.646 | 0.950 | **49.666** | **0.943** | **2.947** |
| | MS (MPa) | 5 | 0.159 | 0.714 | 0.146 | 0.660 | 1.118 |

damage area, absorbed energy, maximum contact force, and maximum stress are 21, 9, 28, and 26, respectively. The number of selected bands accounts for 11.9%, 5.1%, 15.9%, and 14.7% of the total bands, respectively. Most of the characteristic wavebands for each mechanical parameter are different, indicating that the corresponding characteristic information of the spectral variables is different for different mechanical parameters.

*3.5. PLSR Model Results Based on Characteristic Spectral Data and Mechanical Parameters.* In this research, the PLSR models based on the characteristic wavelengths selected by the CARS and the full-wavelength variables are built, respectively. The results are shown in Table 3. As it can be seen from the table, for the prediction of damage area, absorbed energy and maximum contact force, the $R_P$ and RMSEP of the SNV-PLSR model are 0.891 and 102.021 $mm^2$, 0.838 and 1.337 J, and 0.907 and 70.319 N, respectively, and the values of RPD are 2.111, 1.521, and 2.225, respectively. The $R_P$ and RMSEP of the SNV-CARS-PLSR model are 0.920 and 86.452 $mm^2$, 0.845 and 1.303 J, and 0.943 and 49.666 N, respectively. The values of RPD are 2.415, 1.622, and 2.947, respectively. The results show that the SNV-CARS-PLSR model prediction performance based on characteristic wavelengths is better than the SNV-PLSR model prediction performance based on full wavelengths in predicting damage area, absorbed energy, and maximum contact force. However, for the prediction of maximum stress, the SNV-PLSR model prediction accuracy is slightly higher than that of the SNV-CARS-PLSR model. The possible reason for this is that some of the spectral information associated with the maximum stress is removed when the characteristic wavelengths are selected, resulting in the amount of characteristic spectral information input to the model being reduced, thus the prediction accuracy of the model is reduced. Overall, the selection of the characteristic wavelengths affects the prediction accuracy of the PLSR model, and the SNV-CARS-PLSR model based on fewer variables achieves a high prediction accuracy. This indicates that the characteristic wavelengths selected by CARS can replace the full wavelengths. Therefore, the selected characteristic spectral data by CARS is used for the subsequent data analyses.

Figure 8 shows the correlation between the predicted values and the true values of the mechanical parameters, the $X$-axis is the actual measured value and the $Y$-axis is the predicted value. As it can be seen from Figures 8(a)–8(c), all sample points are evenly distributed around the regression line and the sample points are relatively close to the regression line, indicating that the characteristic wavelengths selected based on the CARS method basically cover the characteristic information of the yellow peach damage region. The damage area, absorbed energy, and maximum contact force of yellow peach are well predicted by the PLSR model, indicating there is a strong linear correlation between the spectral data and the mechanical parameters of yellow peach. The $R_P$ and RMSEP of damage area, absorbed energy, and maximum contact force are 0.920 and 86.452 $mm^2$, 0.845 and 1.303 J, and 0.943 and 49.666 N, respectively. It indicates that the mechanical damage area, absorbed energy, and maximum contact force of yellow peach parameters can be accurately predicted by the SNV-CARS-PLSR model. Comparing with the full wavelengths, the 2.8%–8.5% variables of the full-spectrum are used in this model, and the detection efficiency is greatly improved, which is beneficial to practical applications.

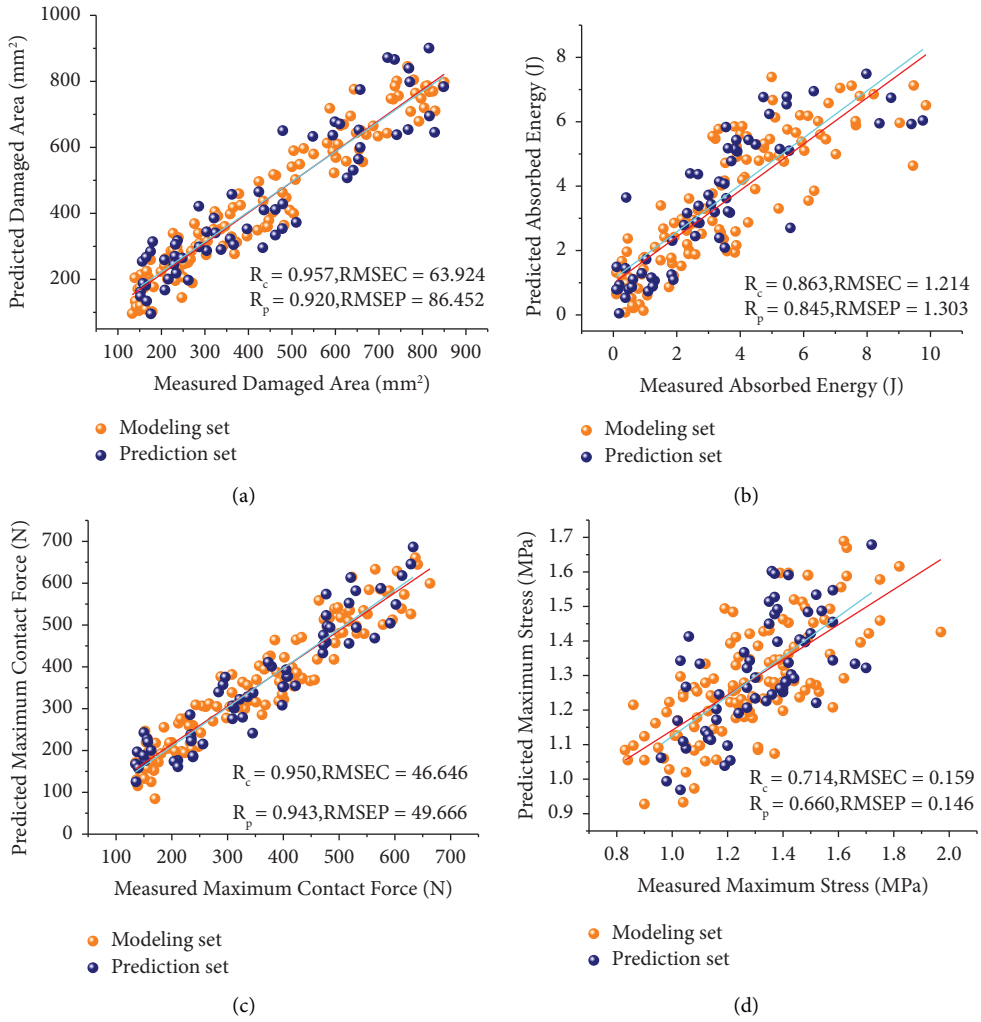


Figure 8: Scatter plot of the modeling set and prediction set: (a) Damaged area; (b) Absorbed energy; (c) Maximum contact force; (d) Maximum stress.

As shown in Figure 8(d), for the prediction of maximum stress, the $R_P$ and RMSEP of the SNV-CARS-PLSR model are 0.660 and 0.146 MPa, respectively, and the accuracy of the prediction of maximum stress can be improved. There are two main reasons for the unsatisfactory forecast results: on the one hand, there are large errors in the calculation process of the maximum stress, on the other hand, the linear correlation between the maximum stress and the spectral data is weak. The PLSR model cannot accurately predict the maximum stress. In future research, a better measurement method of the contact area should be found to reduce the error in the calculation of the maximum stress. Also, the best model for predicting maximum stress is found, or the prediction performance of the PLSR model for maximum stress by combining spectral information with image features is improved.

## 4. Conclusions

In this study, hyperspectral imaging combined with mechanical parameters is used to quantitatively investigate the impact damage of yellow peaches, and the PLSR models between mechanical parameters and spectral variables are established by chemometric methods. During the research, the statistical regression models between the damaged area and other mechanical parameters are established. Then, the raw spectra are preprocessed by SNV, MSC, and SG smoothing. Finally, the CARS is used to select the characteristic wavelengths of the spectral data, and the PLSR model is established based on the spectral data of characteristic bands and full bands. After analysis and comparison, the main conclusions of this study are as follows:

(1) The absorbed energy and maximum contact force of yellow peaches have good linear correlations with the damaged area, and their $R^2$ are 0.83 and 0.90, respectively, which indicates that the maximum contact force and absorbed energy are the optimal mechanical parameters to characterize the impact damage of yellow peaches.

(2) Among the three preprocessing methods, the SNV method has the best preprocessing effect on the original spectral data.

(3) In the PLSR model, the SNV-CARS-PLSR model has the highest prediction accuracy for damage area, absorbed energy, maximum contact force, and maximum stress. The RP and RMSEP of this model are 0.920 and 86.452 $mm^2$, 0.845 and 1.303 J, 0.943 and 49.666 N, and 0.660 and 0.146 MPa, respectively.

In summary, the above research results confirm the potential of NIR hyperspectral imaging technology to quantitatively predict the mechanical parameters of yellow peach. This provides a theoretical basis for quantitatively evaluating the quality and guiding the postharvest handling of yellow peaches.

## Data Availability

The data that support the findings of this study are available upon request from the authors.

## Conflicts of Interest

The authors declare that they have no conflicts of interest.

## Acknowledgments

National Science and Technology Award Backup Project Cultivation Plan (20192AEI91007) and Natural Science Foundation of China (12103019).

## References

[1] R. Lewis, A. Yoxall, M. B. Marshall, and L. A. Canty, "Characterising pressure and bruising in apple fruit," *Wear*, vol. 264, no. 1-2, pp. 37–46, 2008.

[2] J. Xing, V. Van Linden, M. Vanzeebroeck, and J. De Baerdemaeker, "Bruise detection on Jonagold apples by visible and near-infrared spectroscopy," *Food Control*, vol. 16, no. 4, pp. 357–361, 2005.

[3] U. Kitthawee, S. Pathaveerat, T. Srirungruang, and D. Slaughter, "Mechanical bruising of young coconut," *Biosystems Engineering*, vol. 109, no. 3, pp. 211–219, 2011.

[4] L. U. Opara, "Bruise susceptibilities of "Gala" apples as affected by orchard management practices and harvest date," *Postharvest Biology and Technology*, vol. 43, no. 1, pp. 47–54, 2007.

[5] R. Lu, "Detection of bruises on apples using near-infrared hyperspectral imaging," *Transactions of the ASAE*, vol. 46, no. 2, p. 523, 2003.

[6] Q. Zhu, J. Guan, M. Huang, R. Lu, and F. Mendoza, "Predicting bruise susceptibility of "golden delicious" apples using hyperspectral scattering technique," *Postharvest Biology and Technology*, vol. 114, pp. 86–94, 2016.

[7] Y. B. Öztekin and B. Güngör, "Determining impact bruising thresholds of peaches using electronic fruit," *Scientia Horticulturae*, vol. 262, Article ID 109046, 2020.

[8] R. Stopa, D. Szyjewicz, P. Komarnicki, and Ł. Kuta, "Limit values of impact energy determined from contours and surface pressure distribution of apples under impact loads," *Computers and Electronics in Agriculture*, vol. 154, pp. 1–9, 2018.

[9] Z. Stropek and K. Gołacki, "Quantity assessment of plastic deformation energy under impact loading conditions of selected apple cultivars," *Postharvest Biology and Technology*, vol. 115, pp. 9–17, 2016.

[10] Z. Stropek and K. Gołacki, "A new method for measuring impact related bruises in fruits," *Postharvest Biology and Technology*, vol. 110, pp. 131–139, 2015.

[11] X. An, Z. Li, M. Zude-Sasse, F. Tchuenbou-Magaia, and Y. Yang, "Characterization of textural failure mechanics of strawberry fruit," *Journal of Food Engineering*, vol. 282, Article ID 110016, 2020.

[12] R. Moscetti, R. P. Haff, D. Monarca, M. Cecchini, and R. Massantini, "Near-infrared spectroscopy for detection of hailstorm damage on olive fruit," *Postharvest Biology and Technology*, vol. 120, pp. 204–212, 2016.

[13] A. Plaza, J. A. Benediktsson, J. W. Boardman et al., "Recent advances in techniques for hyperspectral image processing," *Remote Sensing of Environment*, vol. 113, pp. S110–S122, 2009.

[14] D. Lorente, N. Aleixos, J. U. A. N. Gómez-Sanchis, S. Cubero, O. L. García-Navarrete, and J. Blasco, "Recent advances and applications of hyperspectral imaging for fruit and vegetable quality assessment," *Food and Bioprocess Technology*, vol. 5, no. 4, pp. 1121–1142, 2012.

[15] W. Tan, L. Sun, F. Yang et al., "Study on bruising degree classification of apples using hyperspectral imaging and GS-SVM," *Optik*, vol. 154, pp. 581–592, 2018.

[16] J. Zhao, A. Sugirbay, Y. Chen et al., "FEM explicit dynamics simulation and NIR hyperspectral reflectance imaging for determination of impact bruises of *Lycium barbarum* L," *Postharvest Biology and Technology*, vol. 155, pp. 102–110, 2019.

[17] Q. Liu, K. Sun, J. Peng, M. Xing, L. Pan, and K. Tu, "Identification of bruise and fungi contamination in strawberries using hyperspectral imaging technology and multivariate analysis," *Food Analytical Methods*, vol. 11, no. 5, pp. 1518–1527, 2018.

[18] L. Pan, Y. Sun, H. Xiao et al., "Hyperspectral imaging with different illumination patterns for the hollowness classification of white radish," *Postharvest Biology and Technology*, vol. 126, pp. 40–49, 2017.

[19] J. Li, X. Rao, and Y. Ying, "Detection of common defects on oranges using hyperspectral reflectance imaging," *Computers and Electronics in Agriculture*, vol. 78, no. 1, pp. 38–48, 2011.

[20] A. López-Maestresalas, J. C. Keresztes, M. Goodarzi, S. Arazuri, C. Jarén, and W. Saeys, "Non-destructive detection of blackspot in potatoes by Vis-NIR and SWIR hyperspectral imaging," *Food Control*, vol. 70, pp. 229–241, 2016.

[21] G. ElMasry, N. Wang, and C. Vigneault, "Detecting chilling injury in red delicious apple using hyperspectral imaging and neural networks," *Postharvest Biology and Technology*, vol. 52, pp. 1–8, 2009.

[22] B. Zhang, S. Fan, J. Li et al., "Detection of early rottenness on apples by using hyperspectral imaging combined with spectral analysis and image processing," *Food Analytical Methods*, vol. 8, pp. 2075–2086, 2015.

[23] S. Fan, C. Li, W. Huang, and L. Chen, "Detection of blueberry internal bruising over time using NIR hyperspectral reflectance imaging with optimum wavelengths," *Postharvest Biology and Technology*, vol. 134, pp. 55–66, 2017.

[24] Y. Liu, M. Cheng, and Y. Hao, "Spectral diagnostic techniques and its application in agricultural quality testing," *Journal of East China Jiaotong University*, vol. 162, no. 4, pp. 1–7, 2018.

[25] P. Zhang, H. Ji, H. Wang, Y. Liu, X. Zhang, and C. Ren, "Quantitative evaluation of impact damage to apples using NIR hyperspectral imaging," *International Journal of Food Properties*, vol. 24, no. 1, pp. 457–470, 2021.

[26] D. Xu, H. Wang, H. Ji et al., "Quantitative evaluation of impact damage to apple by hyperspectral imaging and mechanical parameters," *Food Analytical Methods*, vol. 12, no. 2, pp. 371–380, 2019.

[27] X. Lin and G. H. Brusewitz, "Peach bruise thresholds using the instrumented sphere," *Applied Engineering in Agriculture*, vol. 10, no. 4, pp. 509–513, 1994.

[28] H. Wang, "Marker identification technique for deformation measurement," *Advances in Mechanical Engineering*, vol. 5, Article ID 246318, 2013.

[29] X. Zhang, X. Chu, H. Ji, and Y. Wang, "Effect of freezing rate on the onion cell deformation evaluated by digital image correlation," *Food Analytical Methods*, vol. 9, no. 11, pp. 3125–3132, 2016.

[30] Z. Stropek and K. Gołacki, "Impact characteristics of pears," *Postharvest Biology and Technology*, vol. 147, pp. 100–106, 2019.

[31] A. Rinnan, F. V. D. Berg, and S. B. Engelsen, "Review of the most common pre-processing techniques for near-infrared spectra," *TrAC, Trends in Analytical Chemistry*, vol. 28, no. 10, pp. 1201–1222, 2009.

[32] H. Li, Y. Liang, Q. Xu, and D. Cao, "Key wavelengths screening using competitive adaptive reweighted sampling method for multivariate calibration," *Analytica Chimica Acta*, vol. 648, no. 1, pp. 77–84, 2009.

[33] C. Gomez, P. Lagacherie, and G. Coulouma, "Continuum removal versus PLSR method for clay and calcium carbonate content estimation from laboratory and airborne hyperspectral measurements," *Geoderma*, vol. 148, no. 2, pp. 141–148, 2008.

[34] F. Lu, Y. Ishikawa, H. Kitazawa, and T. Satake, "Impact damage to apple fruits in commercial corrugated fiberboard box packaging evaluated by the pressure-sensitive film technique," *Journal of Food Agriculture and Environment*, vol. 8, no. 2, pp. 218–222, 2010.

[35] S. Yin, X. Bi, Y. Niu, X. Gu, and Y. Xiao, "Hyperspectral classification for identifying decayed oranges infected by fungi," *Emirates Journal of Food and Agriculture*, vol. 29, pp. 601–609, 2017.

[36] R. Lu, H. Cen, M. Huang, and D. P. Ariana, "Spectral absorption and scattering properties of normal and bruised apple tissue," *Transactions of the ASABE*, vol. 53, no. 1, pp. 263–269, 2010.